Article

Journal of
Nanoscience and Nanotechnology
Vol. 14, 6900–6906, 2014
www.aspbs.com/jnn

Ultra-Dispersed Pt Nanoparticles on SAPO-34/γ-Al_2O_3 Support for Efficient Propane Dehydrogenation

Yue Chu, Qiang Zhang*, Tongwei Wu, Zeeshan Nawaz, Yao Wang*, and Fei Wei*

Beijing Key Laboratory of Green Chemical Reaction Engineering and Technology, Department of Chemical Engineering, Tsinghua University, Beijing 100084, P. R. China

Ultra-dispersed precious metal nanoparticles with good thermal stability are highly required for heterogeneous catalysis. However, the efficient and effective strategy to disperse ultra-fine precious metal nanoparticles at high reaction temperature is still not fully understood yet. In this contribution, a family of catalysts with ultra-small Pt nanoparticles were prepared using impregnation method by adjusting the zeolite content in the SAPO-34 and γ-Al_2O_3 mixed support. The effect of Pt nanoparticle size on the catalytic activity, selectivity, and stability was investigated in the propane dehydrogenation reaction. Catalyst with smaller Pt particles exhibits better catalytic performance. Both the highest Pt dispersion and the best catalytic activity can be achieved by using SAPO-34 and γ-Al_2O_3 mixed support with 70 wt.% of SAPO-34. The size and structure of the Pt nanoparticles on the optimal catalyst were characterized by transmission electron microscopy. Pt nanoparticles with an average size of 1.32 nm were observed. There were stronger metal-support interactions between the oxidized tin species and Pt particles on SAPO-34 support compared to that on γ-Al_2O_3 catalyst. These lead to high Pt dispersion and consequently good catalytic performance.

Keywords: Pt, Nanoparticle, Support, SAPO, Dehydrogenation, Catalysis.

1. INTRODUCTION

Platinum is an important catalyst, being used on a large scale for petroleum refining, automobile exhaust conversion, carbon monoxide oxidation, dehydrogenation and hydrogenation processes, and so on.[1–6] As platinum is high cost but with high activity. Therefore, only small amount of them, often less than 1 wt%, will be used as the catalytic material. This requires for high dispersion of the metal nanoparticles on the support. The smaller the particles, the larger the fraction of metal atoms that are exposed at surfaces, where they are accessible to reactant molecules and available for catalysis.

Supporting of platinum on a porous support provides an efficient way to obtain highly dispersed catalyst. The pores serve as high-area internal platforms for the metal particles, and steric confinement for particle aggregation. The interaction between platinum and the support further hinders the movement of metal nanoparticles and increases its stability. Usually, another metal (such as Sn, Fe, Ga) is added to the catalyst as a promoter to improve the dispersion of platinum in terms of geometric and/or electronic effects.[7–9] Conventional supports are metal oxide like γ-Al_2O_3, for example, Pt–Sn/γ-Al_2O_3 catalyst used in Oleflex process for propane dehydrogenation, and Pt–Re/γ-Al_2O_3 catalyst used in catalytic reforming process.[10, 11]

In the past few decades, extensively exploration in zeolite applications in chemical industry brings breakthrough in noble metal supported catalyst.[12–14] The zeolite affords large surface area, uniform pore diameter, and adjustable acidic strength when it used as catalyst support. For example, for propane dehydrogenation reaction, Beta, L-zeolite, Y-zeolite, SBA-15, ZSM-5, SAPO-34 were used as catalyst support instead of γ-Al_2O_3 and these zeolite-based Pt catalysts were reported to be much more active, selective and stable than the classical Al_2O_3 based catalysts.[15–18]

Pt-based catalyst is widely used in propane dehydrogenation to propylene process. Propylene is an indispensable raw material in the production of polypropylene, acrolein, acrylonitrile, and acrylic acid. Propylene has been produced mainly by conventional cracker such as steam and fluid catalytic crackers as a by-product. Nowadays, on-purpose propylene production technologies such as propane dehydrogenation have received a great deal of attention due to their potential to make-up the shortfall of propylene supply left by conventional crackers. High

*Authors to whom correspondence should be addressed.

 1533-4880/2014/14/6900/007 doi:10.1166/jnn.2014.8956

Pt dispersion, good thermal and hydrothermal stability are urgently required for propane dehydrogenation reaction at high temperature. During our continuing interest in the propane dehydrogenation process, SAPO-34 zeolite was considered to be an appropriate support for Pt-based catalyst used in propane dehydrogenation process. SAPO-34 is a silicoaluminophosphate zeolite with chabazite (CHA) topology possessing good thermal stability. Besides, its Si based acid sites render it resistant to hydrothermal treatment and exhibit moderate acidic strength compared to its aluminosilicate counterpart.[13, 19–21] Pt-based catalyst with SAPO-34 support and Sn as promoter is reported to be with fairly good propane dehydrogenation activity and stability. Al_2O_3 addition to the support improves the Pt dispersion and catalytic performance.[22, 23] However, the influence of support composition in the SAPO-34 and Al_2O_3 mixed support was not fully investigated yet. The mechanism of Pt dispersion on SAPO-34 included support was not fully understood.

In this contribution, a series of Pt nanoparticles of different sizes supported on SAPO-34 and Al_2O_3 mixed support were prepared by adjusting the composition of the support. The effect of Pt particle size on the catalytic performance was investigated systemically. Catalyst with the highest Pt dispersion is characterized with high-resolution transmission electron microscopy (HR-TEM), X-ray photoelectron spectroscopy (XPS), and H_2-temperature programmed reduction (H_2-TPR). The particle size distribution (PSD) of the highly dispersed Pt nanoparticles and their fine structure are explored. Strong metal-support interaction is directly observed in XPS and H_2-TPR experiment.

2. EXPERIMENTAL DETAILS

2.1. Catalyst Synthesis

The zeolite SAPO-34 was prepared according to the procedure reported in the literatures.[23–25] The SAPO-34 was dispersed into an alumina matrix prepared from pseudoboehmite as follow: The SAPO-34 and the pseudoboehmite was suspended in 20 mL distilled water, followed by depressurized evaporation of the resulting slurry at 343 K and then overnight drying at 383 K. After drying, the solid mixture was calcined in air at 873 K for 5 h. The as-obtained products were labelled as SAPO-34(x)–Al, (x is the mass fraction of SAPO-34, $x = 0$, 30, 50, 70, 90, 100 wt.%).

Pt–Sn/SAPO-34(x)–Al was prepared by consecutive impregnation of Sn followed by Pt. The Sn/SAPO-34–Al was prepared by incipient wetness impregnation. Firstly, appropriate amounts of $SnCl_2 \cdot 2H_2O$ (Aladdin, 99.99%) was dissolved in deionized water, and the resulting solution (0.15 mol/L) was added dropwise to the SAPO-34–Al support to ensure 1 wt.% Sn component in the catalyst. The as-obtained catalyst was dried at 383 K for 3.0 h and finally calcined at 773 K for 3.5 h. After that, $H_2PtCl_6 \cdot 6H_2O$ (Aladdin, 99.5%) was used as precursor for Pt impregnation. The procedure was similar to that of Sn impregnation. The amount of the 0.03 mol/L H_2PtCl_6 aqueous solution was controlled to give a 0.5 wt.% Pt component in the final catalyst.

2.2. Catalyst Characterization

XRD pattern of the Pt–Sn/SAPO-34(x)–Al catalyst were obtained by a Rigaku D/Max-rB diffractometer with Cu K_α radiation with scan range 3~70°. The element contents were determined by inductively coupled plasma-atomic emission spectrometry (ICP-AES). The measurements were performed with a VISTA-MPX inductively coupled plasma quantometer, and the sample was dissolved in a mixture of HF/HNO_3. The H_2-chemisorption experiments were carried on using Chembet PULSAR TPR/TPD (*p*/*n* 02139-1) (Quantachrome Instruments Corporation). About 50 mg of Pt–Sn/SAPO-34(x)–Al was loaded into a quartz cell and then reduced in flowing 7% H_2/Ar (10 mL/min). The temperature of the sample was raised at 5 K/min to 773 K and then maintained for 2.0 h. The sample was then flushed in flowing Ar at 813 K for 2.0 h and then cooled down to 318 K. The uptake of chemisorbed H_2 was then measured by determining the uptake of H_2 from pulses of 4% H_2/Ar using a TCD detector. The pulse size was 1 mL/g and the time between pulses was 5 min. A JEOL 2010F microscopy operated at 120 kV was employed to acquire the TEM images. A sacrificial-zeolite specimen preparation technique is developed for the electron microscope analysis of the Pt nanoparticle on the catalysts.[26] The surface characterization was performed by using an Escalab 250 xi X-ray photoelectron spectroscopy (XPS). Binding energy is calibrated with C $1s = 284.8$ eV. Temperature programmed reduction (TPR) was measured with the same apparatus as that of H_2-chemisorption. Prior to the TPR experiments, the catalysts were dried in flowing Ar at 773 K for 1 h. 7% H_2/Ar (10 mL/min) was used as the reducing gas. The rate of temperature rise in the TPR experiment was 5 K/min up to 923 K.

2.3. Catalytic Performance Evaluation

The catalyst performance testing was performed in a fixed bed quartz reactor at 863 K over 200 mg catalyst. The catalyst was firstly reduced with H_2 at 773 K for 3 h before in the introduction of feeding gas. The $WHSV_{C3H8}$ was 2.8 h^{-1} and the molar ratio of H_2/C_3H_8 in feed gas was 0.25. The analysis of the product was performed on a gas chromatograph (GC) (TechComp 7890II) equipped with 50 m PLOT Al_2O_3 capillary column and FID detector.

3. RESULTS AND DISCUSSION

3.1. Catalysts with Pt Nanoparticles of Different Sizes

3.1.1. Catalyst Characterization

The XRD pattern of the reduced Pt–Sn/SAPO-34(x)–Al is shown in Figure 1. The chabazite (topology style of

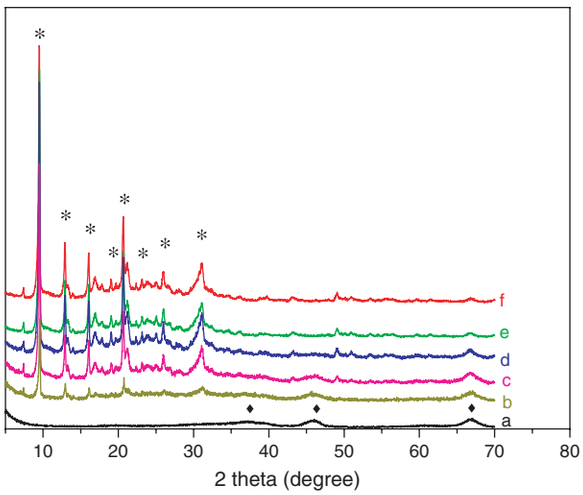

Figure 1. X-ray diffraction patterns of (a) Pt–Sn/Al_2O_3, (b) Pt–Sn/SAPO-34(30)–Al, (c) Pt–Sn/SAPO-34(50)–Al, (d) Pt–Sn/SAPO-34(70)–Al, (e) Pt–Sn/SAPO-34(90)–Al, (f) Pt–Sn/SAPO-34. (*) chabazite and (♦) γ-Al_2O_3.

SAPO-34) diffraction lines and the γ-Al_2O_3 diffraction lines are clearly observed, indicating that the structure of zeolite and Al_2O_3 were well preserved after the impregnation procedure. There is no XRD evidence for the presence of crystalline Pt and Sn phases because of the very low loading content.

Table I presents the element composition and Pt dispersion based on the irreversible uptake of H_2-chemisorption using an adsorption stoichiometry of unity between hydrogen and platinum in the catalysts. Hemispherical particle size is determined from d (nm) $= 1.13/D$, where D is the metallic dispersion. The calculated particle sizes are listed in the last column of the table. From the experimental results, SAPO-34 is suggested to be a good material for Pt particles supporting as catalysts which possess SAPO-34 in the support exhibit improvement in Pt dispersion than catalyst with pure Al_2O_3 as support. Besides that, the composition of the SAPO-34 and Al_2O_3 mixed support plays a decisive role in the dispersion of Pt nanoparticles. The relationship between the fraction of SAPO-34 in the support and the Pt dispersion is not monotonic, with the maximum dispersion exists in the Pt–Sn/SAPO-34(70)–Al catalyst. The support composition plays critical role on the catalytic performance, which is widely detected in heterogeneous catalysis processes.[27–29] The active size distribution (such as Pt nanoparticles), and its strong metal-support interaction were explored to shed a light on its reactivity on dehydrogenation.

Table I. Basic characterization of the catalysts.

Catalysts	Element content (wt%)[a] Pt	Sn	D_{Pt} (%)[b]	D_p (nm)[c]
Pt–Sn/Al_2O_3	0.41	0.97	8.6	13.07
Pt–Sn/SAPO-34(30)–Al	0.40	1.01	18.2	6.22
Pt–Sn/SAPO-34(50)–Al	0.39	0.94	35.5	3.19
Pt–Sn/SAPO-34(70)–Al	0.40	1.03	83.9	1.35
Pt–Sn/SAPO-34(90)–Al	0.43	1.04	61.0	1.85
Pt–Sn/SAPO-34	0.41	0.98	47.3	2.39

Notes: [a]Results from ICP-AES analysis; [b]Measured by H_2-chemisorption; [c]Determined by D_p (nm) $= 1.13/D_{Pt}$.

3.1.2. *Effect of Pt Nanoparticle Sizes on Catalytic Performance in Propane Dehydrogenation*

Figure 2 shows the catalytic performance of catalysts with different supports in the propane dehydrogenation reaction. Propane conversion and selectivity of the main product, propylene, vary significantly with the composition of the support. Catalyst with the highest Pt dispersion, Pt–Sn/SAPO-34(70)–Al, exhibits the best catalytic activity and stability. An initial conversion of 35.3% is achieved on Pt–Sn/SAPO-34(70)–Al catalyst. Figure 3 shows the variation of catalytic activity with time on stream on different Pt nanoparticles. This relationship is summarized based on the experimental results shown in Figure 3. The catalyst

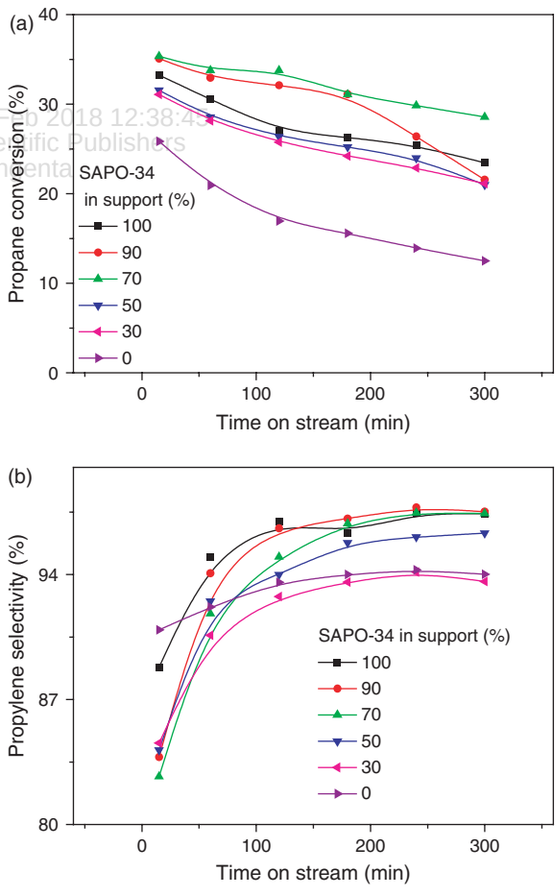

Figure 2. Catalytic performance of Pt–Sn/SAPO-34(x)–Al catalysts in the propane dehydrogenation at 863 K. (a) propane conversion, (b) propylene selectivity.

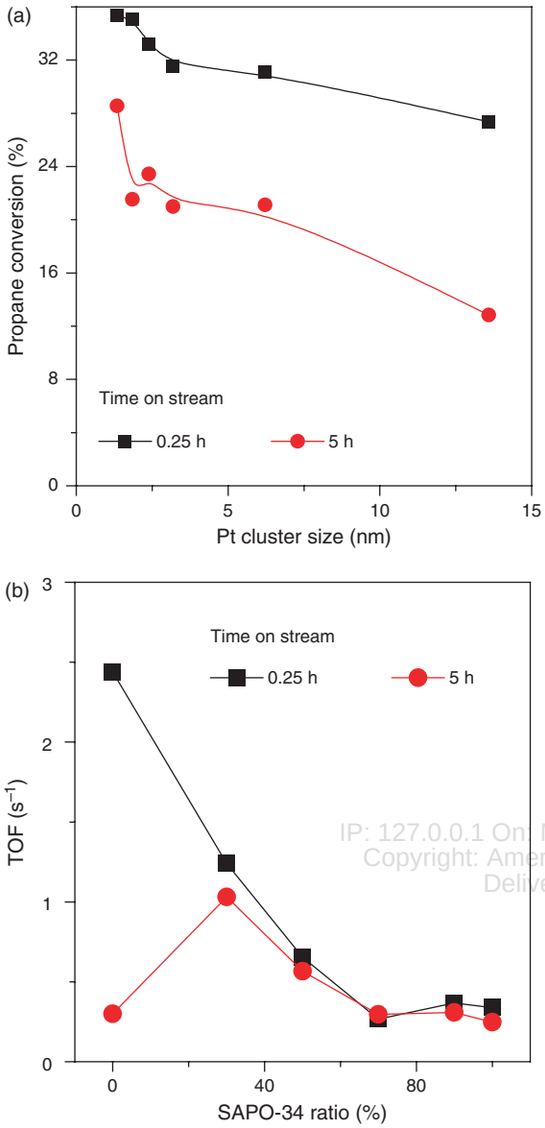

Figure 3. (a) Variation of catalytic activity with Pt particle size at different times on stream in propane dehydrogenation at 863 K; (b) TOF of Pt–Sn/SAPO-34–Al_2O_3 of different support compositions.

with smaller Pt particle size possesses better catalytic activity and stability (Fig. 3(a)). The turnover frequency (TOF) based on Pt catalyst decreased with more SAPO-34 addition. However, the TOF on Pt/Al_2O_3 decreased rapidly, while the addition of SAPO-34 support benefit for its reactivity preservation. A highest TOF of 1.03 s^{-1} can be observed on Pt–Sn/SAPO-34(30)–Al at a time stream of 5 h, while a value of 0.29 s^{-1} was detected on Pt–Sn/SAPO-34(30)–Al catalyst.

The influence of Pt particle size on the dehydrogenation activity has been further investigated in other catalysts with different supports.[4, 7, 30–33] The relationship between the Pt particle size and catalytic performance has been reported. Somorjai et al.[34] claimed that atomic height steps and kinks on platinum surfaces were distinct catalytic sites where C—C, C—H, and H—H bond scissions occurred during the reactions of hydrocarbon. Small Pt particles possessed larger step density and thus higher catalytic activity. Santen found that dehydrogenation involved activation of σ chemical bonds.[35] The activation proceeded at a single metal atom; therefore the reaction rate largely depended on coordinative unsaturation of reactive surface atoms which is abundant in highly dispersed Pt particles. The activation barrier for C—H cleavage was much smaller than that for C—C cleavage on small Pt clusters through quantum chemical calculations, explaining the better propylene selectivity of smaller Pt particles.[36] Based on these investigations, it is suggested that the catalytic performance is the direct representation of the Pt dispersion. The high Pt dispersion on the Pt–Sn/SAPO-34(70)–Al catalyst is further demonstrated by the catalyst testing results.

3.2. Highly Dispersed Pt Nanoparticles

3.2.1. Characterization of the Pt Nanoparticles

The Pt-Sn/SAPO-34(70)-Al catalyst with the highest Pt dispersion is characterized with HR-TEM to obtain the particle size distribution (PSD) and the nanostructure of the Pt nanoparticles. Figure 4 shows TEM images of the catalyst, the corresponding EDS results and the PSD of the Pt nanoparticles. The low magnification TEM images (Fig. 4(a)) shows the cubic SAPO-34 with crystal size of 1.2 μm together with γ-Al_2O_3 particles adhered to its external surface. From its EDS spectra shown in Figure 4(c), elements of Pt, Sn, Si, Al, P, O, Cl were found. The Cl element is the residual from the metal precursor. The ratio of Al to P further indicates that γ-Al_2O_3 adheres on the external surface of the zeolite as the Al and P atoms are of the same amount in the SAPO-34 zeolite. Highly dispersed Pt particles were observed by high resolution TEM images on the edge of the support (central parts are too thick for high resolution TEM observation). A typical image is shown in Figure 4(b). The histogram of PSD (Fig. 4(d)) was constructed from the TEM images whereby 306 particles were counted. The mean particle size was estimated to be 1.32 ± 0.04 nm. This is in agreement with the result measured by H_2-chemisorption. The nanostructure of the Pt particles is further investigated in detail. Figure 5 illustrates high resolution TEM images of typical Pt particles with different crystal faces, the indicated reflections in the fast Fourier transform (FFT) of the particles, as well as further inverse FFT of the reflections. The interplanar distance determined from the inverse FFT images is 0.228, 0.272, 0.382 nm, which correspond well to the (111), (110), (100) crystal faces of Pt, respectively.

3.2.2. Strong Metal-Support Interaction

For supported metal catalysts, the strength of metal-support interaction plays an important role in the metal dispersion. If the interaction is weak, the metal particles easily sinter to form large ones at high temperature. While

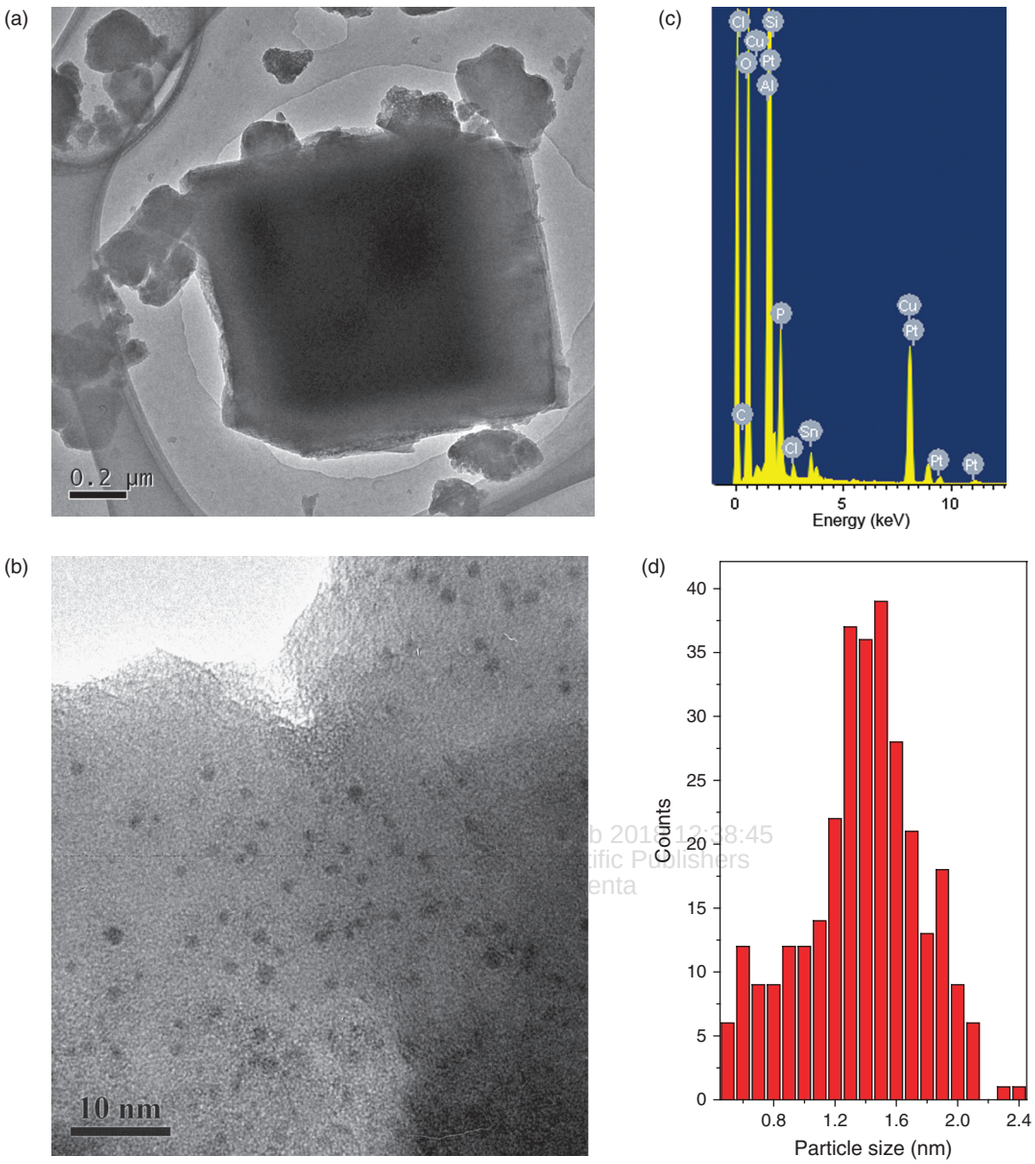

Figure 4. TEM images of the Pt–Sn/SAPO-34(70)–Al at different magnifications and the EDS spectra. (a) (b) TEM images at different magnifications. (c) Its corresponding EDS spectra. (d) The histogram of PSD of Pt particles from the TEM images.

if strong metal-support interaction exists, small metal particles are anchored to the support firmly, leading to high metal dispersion.[37, 38] For Pt–Sn bimetallic catalyst, the surface structure and metal-support interaction are much more complicated than that of the mono metallic catalysts. Both the second component (Sn) and the support influence the dispersion of Pt. Lin et al.[39] investigated the structure of the Pt–Sn/Al_2O_3 catalyst and found that the second component remained oxidized after reduction and the tendency of its mono layer distribution would partially modify the surface of the support. Pt particles which located on the second component own higher dispersion due to the geometric effect and provided major contribution to the dehydrogenation reaction.

The surface characterization of the Pt–Sn/SAPO-34(70)–Al catalyst is carried out by XPS and H_2-TPR in comparison with the conventional Pt–Sn/γ–Al_2O_3 catalyst. XPS spectra of Sn $3d_{5/2}$ level of the two catalysts are shown in Figure 6. The Pt 4f lines are difficult to analyze for the reason that these lines are overlapped by the Al 2p lines and the Pt 4d lines are too weak, as a result, the XPS spectra is not fitted for further determination of the Pt species. From the deconvolution of the XPS spectra of the Sn $3d_{5/2}$ level for the bimetallic Pt–Sn samples, peaks at 487.2–487.6 eV are available, indicating that Sn remains in oxidation state. This is in agreement with the results of other reports.[39–41] Pt–Sn/SAPO-34(70)–Al shows slightly higher Sn $3d_{5/2}$ binding energy value with respect to that

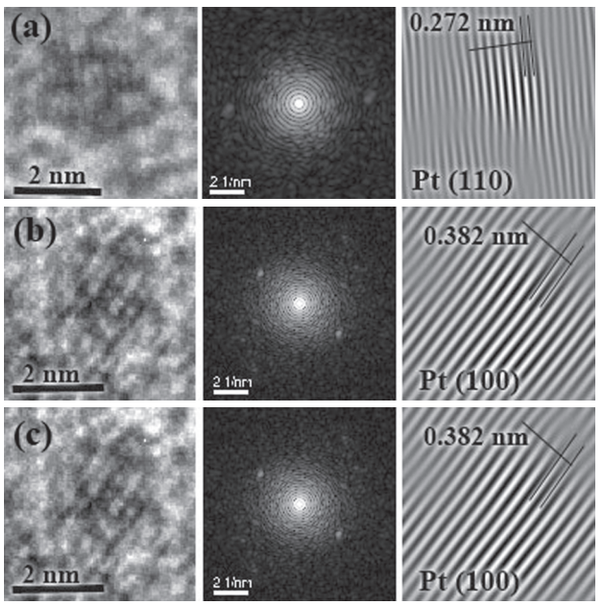

Figure 5. HRTEM image of the Pt particle, its indicated reflection in the Flourier transform (FFT) and inverse FFT of the reflection of (a) (111) crystal face, (b) (110) crystal face, (c) (100) crystal face.

of conventional Pt–Sn/γ–Al_2O_3 catalyst. Such shift could be due to stronger interaction with the mixture support. This is benefit for the mono layer distribution of Sn on the support and then its geometric and/or electronic effect to the Pt centres would be more significant, leading to higher Pt dispersion and better catalytic activity.

The strong Sn-support interaction exists in the Pt–Sn/SAPO-34(70)–Al catalyst is related to a special interaction between Sn species and the SAPO-34 zeolite. The SAPO-34 zeolite is made up of Si, Al, P, O elements. Support contains Al is widely used for Pt–Sn based catalysts.[32, 42, 43] Some Si, Al-containing mesoporous and microporous materials are developed to be support for

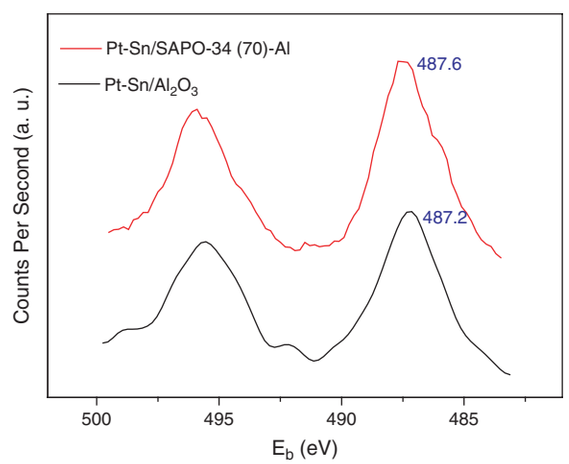

Figure 6. XPS spectra of Sn $3d_{5/2}$ level for the Pt–Sn/SAPO-34(70)–Al and Pt-Sn/Al_2O_3 catalyst.

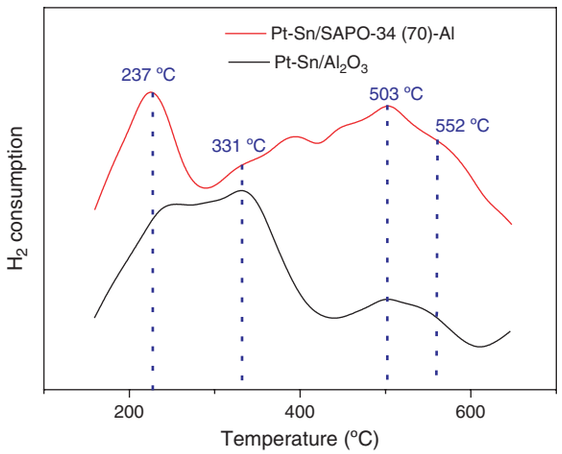

Figure 7. TPR profiles of the Pt–Sn/SAPO-34(70)–Al and Pt–Sn/Al_2O_3 catalyst.

Pt–Sn catalyst.[7, 16, 31, 44–46] Herein, it is supposed that the Si and/or P elements possess strong ability for the mono layer distribution of Sn.

H_2-TPR profiles of the Pt–Sn/SAPO-34 (70)–Al and Pt–Sn/γ-Al_2O_3 are shown in Figure 7. Four reduction peaks are observed for Pt–Sn/γ-Al_2O_3 catalyst: peaks around 237, 331, 503, 552 °C. The peaks around 237 and 503 °C are assigned to be reduction peaks of Pt, while peaks around 331 and 552 °C correspond to reduction peaks of Sn according to reported results.[33, 47] For the two Pt reduction peaks, the latter peak corresponding to a higher reduction temperature indicates a proportion of Pt species strongly interacts with the support. Comparing the areas of the two peaks, it is clearly seen that the proportion of Pt species in strong interaction with the support is small, while most Pt particles are in weak interaction with the support. For Pt–Sn/SAPO-34(70)–Al catalyst, reduction peaks at 227 and 504 °C are assigned to be reduction peaks of Pt, in which the one at high temperature represents the reduction of Pt in strong interaction with the support. Comparing the two TPR curves, the proportion of Pt particles which are in strong interaction is much higher for Pt–Sn/SAPO-34(70)–Al catalyst than the other one, leading to higher Pt dispersion. Based on the investigation of Lin et al.[39] Pt species reduced at high temperature are located on the second metallic component (Sn) modified support, forming "sandwich structure." The higher proportion of Pt particles owning this structure indicates that the Sn species are well distributed on the support, which is in accord with the XPS characterization result of Sn.

4. CONCLUSIONS

By adjusting the fraction of SAPO-34 in the SAPO-34 and Al_2O_3 mixed support, Pt nanoparticles of different sizes are prepared. SAPO-34 included catalysts exhibit better Pt dispersion than catalyst with pure Al_2O_3 as support. The catalyst testing results under the propane dehydrogenation

reaction show that the catalytic activity is sensitive to the Pt particle size, smaller Pt particle leads to better activity and stability. The optimal catalyst with the highest Pt dispersion is characterized using high resolution-TEM to investigate the PSD of the Pt particles and their nanostructure. The average particle size is 1.32 ± 0.04 nm. This catalyst with high Pt dispersion exhibits good propane dehydrogenation activity, selectivity and stability. The Sn species are in oxidation state and strong interaction with the support, benefit for its mono layer distribution on the support. H_2-TPR experimental results show that the higher proportion of Pt particles which are in strong interaction with the support in the SAPO-34 contained catalyst leading to higher Pt dispersion. Such high dispersed Pt catalyst affording promising reactivity for petroleum refining, automobile exhaust conversion, dehydrogenation and hydrogenation reaction.

Acknowledgments: This work was supported by National Basic Research Program of China (973 Program, 2011CB932602), and Natural Scientific Foundation of China (21006056).

References and Notes

1. P. Cong, R. D. Doolen, Q. Fan, D. M. Giaquinta, S. Guan, E. W. McFarland, D. M. Poojary, K. Self, H. W. Turner, and W. H. Weinberg, *Angew. Chem. Int. Ed.* 38, 483 (**1999**).
2. C. Xu, Y. L. Tsai, and B. E. Koel, *J. Phys. Chem.* 98, 585 (**1994**).
3. K. Fujimoto, M. Kameyama, and T. Kunugi, *J. Catal.* 61, 7 (**1980**).
4. V. Galvita, G. Siddiqi, P. Sun, and A. T. Bell, *J. Catal.* 271, 209 (**2010**).
5. F. Zaera and G. Somorjai, *J. Am. Chem. Soc.* 106, 2288 (**1984**).
6. H. W. Lee, J. K. Jeon, K. E. Jeong, S. Y. Jeong, J. Han, B. Seo, S. H. Joo, and Y. K. Park, *J. Nanosci. Nanotechnol.* 13, 6074 (**2013**).
7. M. Santhosh Kumar, D. Chen, A. Holmen, and J. C. Walmsley, *Catal. Today* 142, 17 (**2009**).
8. A. D. Ballarini, P. Zgolicz, I. M. J. Vilella, S. R. De Miguel, A. A. Castro, and O. A. Scelza, *Appl. Catal. A* 381, 83 (**2010**).
9. M. Q. Zhao, Q. Zhang, J. Q. Huang, and F. Wei, *Adv. Funct. Mater.* 22, 675 (**2012**).
10. M. Bhasin, J. McCain, B. Vora, T. Imai, and P. Pujado, *Appl. Catal. A* 221, 397 (**2001**).
11. M. F. L. Johnson and V. LeRoy, *J. Catal.* 35, 434 (**1974**).
12. H. C. Xin, X. P. Li, L. Chen, Y. Huang, G. R. Zhu, and X. B. Li, *Energy and Environment Focus* 2, 18 (**2013**).
13. Y. Cui, Q. Zhang, J. He, Y. Wang, and F. Wei, *Particuology* 11, 468 (**2013**).
14. X. A. Zhang, J. Y. Fang, J. D. Sun, H. Qin, S. L. Chang, and S. Q. Qin, *J. Nanosci. Nanotechnol.* 13, 2589 (**2013**).
15. P. L. De Cola, R. Gläser, and J. Weitkamp, *Appl. Catal. A* 306, 85 (**2006**).
16. L. Bai, Y. Zhou, Y. Zhang, H. Liu, X. Sheng, and Y. Duan, *Catal. Comm.* 10, 2013 (**2009**).
17. M. Santhosh Kumar, A. Holmen, and D. Chen, *Micropor. Mesopor. Mat* 126, 152 (**2009**).
18. Z. Nawaz and F. Wei, *Ind. Eng. Chem. Res.* 52, 346 (**2013**).
19. B. M. Lok, C. A. Messina, R. L. Patton, R. T. Gajek, T. R. Cannan, and E. M. Flanigen, *J. Am. Chem. Soc.* 106, 6092 (**1984**).
20. N. Katada, K. Nouno, J. K. Lee, J. Shin, S. B. Hong, and M. Niwa, *J. Phys. Chem. C* 115, 22505 (**2011**).
21. J. W. Jun, J. Jeon, C. U. Kim, K. E. Jeong, S. Y. Jeong, and S. H. Jhung, *J. Nanosci. Nanotechnol.* 13, 2782 (**2013**).
22. Z. Nawaz, X. Tang, Q. Zhang, D. Wang, and W. Fei, *Catal. Comm.* 10, 1925 (**2009**).
23. Z. Nawaz, Y. Chu, W. Yang, X. Tang, Y. Wang, and F. Wei, *Ind. Eng. Chem. Res.* 49, 4614 (**2010**).
24. J. Zhu, Y. Cui, Y. Wang, and F. Wei, *Chem. Commun.* 3282 (**2009**).
25. Y. Chen, H. Zhou, J. Zhu, Q. Zhang, Y. Wang, D. Wang, and F. Wei, *Catal. Lett.* 124, 297 (**2008**).
26. Y. Chu, W. Zhang, Q. Zhang, Y. Wang, D. S. Su, and F. Wei, *Micropor. Mesopor. Mat* 169, 201 (**2013**).
27. Y. Zhang, Y. Zhou, A. Qiu, Y. Wang, Y. Xu, and P. Wu, *Ind. Eng. Chem. Res.* 45, 2213 (**2006**).
28. K. Honda, X. Chen, and Z. G. Zhang, *Appl. Catal. A* 351, 122 (**2008**).
29. D. Solís, A. L. Agudo, J. Ramírez, and T. Klimova, *Catal. Today* 116, 469 (**2006**).
30. O. A. Bariås, A. Holmen, and E. A. Blekkan, *J. Catal.* 158, 1 (**1996**).
31. M. Santhosh Kumar, D. Chen, J. C. Walmsley, and A. Holmen, *Catal. Comm.* 9, 747 (**2008**).
32. G. Siddiqi, P. Sun, V. Galvita, and A. T. Bell, *J. Catal.* 274, 200 (**2010**).
33. Y. Zhang, Y. Zhou, A. Qiu, Y. Wang, Y. Xu, and P. Wu, *Catal. Comm.* 7, 860 (**2006**).
34. G. Somorjai and D. Blakely, *Nature* 258, 580 (**1975**).
35. R. A. Van Santen, *Accounts. Chem. Res.* 42, 57 (**2008**).
36. S. Vajda, M. J. Pellin, J. P. Greeley, C. L. Marshall, L. A. Curtiss, G. A. Ballentine, J. W. Elam, S. Catillon-Mucherie, P. C. Redfern, and F. Mehmood, *Nat. Mater.* 8, 213 (**2009**).
37. B. Gates, *Chem. Rev.* 95, 511 (**1995**).
38. J. Liu, *Chem. Cat. Chem.* 3, 934 (**2011**).
39. L. Lin, W. Yang, J. Jia, Z. Xu, T. Zhang, Y. Fan, Y. Kou, and J. Shen, *Sci. China Ser. B* 42, 571 (**1999**).
40. K. Balakrishnan and J. Schwank, *J. Catal.* 127, 287 (**1991**).
41. S.-B. He, W.-J. Bi, Y.-L. Lai, X. Rong, X. Yang, and C.-L. Sun, *J. Fuel Chem. Technol.* 38, 452 (**2010**).
42. N. Martín, M. Viniegra, R. Zarate, G. Espinosa, and N. Batina, *Catal. Today* 107–108, 719 (**2005**).
43. X. Zhong, J. Zhu, and J. Liu, *J. Catal.* 236, 9 (**2005**).
44. M. Machida and T. Watanabe, *Appl. Catal. B* 52, 281 (**2004**).
45. M. Santhosh Kumar, A. Holmen, and D. Chen, *Micropor. Mesopor. Mat* 126, 152 (**2009**).
46. B. K. Vu, S. M. Bok, I. Y. Ahn, and E. W. Shin, *Catal. Lett.* 133, 376 (**2009**).
47. L. R. Raddi de Araujo and M. Schmal, *Appl. Catal. A* 235, 139 (**2002**).

Received: 1 December 2012. Accepted: 1 June 2013.